Geophys. J. Int. (2003) **154,** F9–F14

FAST TRACK PAPER

First evidence of post-seismic deformation in the central Mediterranean: Crustal viscoelastic relaxation in the area of the 1980 Irpinia earthquake (Southern Italy)

G. Dalla Via,[1] G. De Natale,[2] C. Troise,[2] F. Pingue,[2] F. Obrizzo,[2] R. Riva[3] and R. Sabadini[1*]

[1] *Dipartimento di Scienze della Terra, Sez. Geofisica, Universitá di Milano, Italy. E-mail: roberto.sabadini@unimi.it*
[2] *Osservatorio Vesuviano, Istituto Nazionale di Geofisica e Vulcanologia, Napoli, Italy*
[3] *DEOS, Faculty of Aerospace Engineering, Delft University of Technology, Netherlands*

Accepted 2003 May 16. Received 2003 May 16; in original form 2002 December 10

SUMMARY

Comparison between measured vertical displacements obtained from two levelling campaigns performed in 1981 and 1985 in the epicentral area of the 1980 Irpinia earthquake (M^S = 6.9) and predictions from viscoelastic Earth models reveal the occurrence of post-seismic deformation due to stress relaxation in the ductile part of the crust. Two regions of broad uplift and subsidence, accumulated during the time interval, characterize the deformation pattern in the footwall and hangingwall of the major fault. The spatial wavelength of the deformation pattern favours relaxation occurring in the lower crust rather than in a weak upper-mantle: the uplift in the footwall explains the 30 mm of upwarping of the crust measured along the levelling line crossing the area where the fault pierces the Earth's surface.

Key words: deformation, Irpinia earthquake, viscoelasticity.

1 INTRODUCTION

Co-seismic deformation at the Earth surface is caused by the instantaneous, elastic release of stress in the fault zone. Immediately after the occurrence of the earthquake, the mechanism of stress release due to viscous flow in the ductile part of the Earth crust starts to operate, leading to post-seismic deformation. This process has been generally studied for large, deep earthquakes, in either thrust or strike slip environments (Pollitz *et al.* 1998; Piersanti 1999). The present study tests the mechanism of stress relaxation in the ductile parts of the crust after the occurrence of a shallow, normal fault event in the Mediterranean region, the 1980 Irpinia earthquake. The joint study of local and worldwide seismological data, static deformations and geological observations provides a detailed picture of the complex mechanism of this event (Westaway & Jackson 1984; De Natale *et al.* 1988; Bernard & Zollo 1989; Pantosti & Valensise 1990; Pingue & De Natale 1993). The main event consisted of three distinct subfaults at least, ruptured at intervals of about 20 s from each other. Surface faulting linked to this earthquake was evident at several places, in particular on the main fault (first subevent), where dislocations up to 1.2 m were observed. The total seismic moment inferred for this event is 3×10^{19} Nm. The estimated seismic moment appeared very stable (to within 20 per cent) for both long and short period seismic data, within a very large range of distances, from local to teleseismic. The total moment estimated from fault models tuned to fit geodetic data is also indistinguishable with respect to the seismologically inferred one, as shown by Pingue *et al.* (1993). Their model, obtained by inverting the co-seismic vertical displacement data in agreement with available seismological observations, is used as the reference for the present study.

* Corresponding author: Dipartimento di Scienze della Terra, Sez. Geofisica - via Cicognara 7 - 20129 Milano - Italy.

2 THE VISCOELASTIC DEFORMATION MODEL AND EARTHQUAKE PARAMETERS

Asymptotic expressions for the fundamental solutions of an incompressible, self-gravitating, spherical, viscoelastic Earth for high harmonic degree are derived by Riva & Vermeersen (2002). These expressions allow us to sum 40 000 spherical harmonic contributions to the predicted co-seismic signal and 6,000 contributions to the post-seismic signal, which guarantees the attainment of convergence both in the co-seismic and post-seismic components. Our predictions have been applied to the modelling of post-seismic vertical displacements measured in the 4-yr period 1981–1985, corresponding to the time interval between the levelling campaigns. The

Table 1. Viscoelastic model parameters (UC = upper crust; LC = lower crust; LCB = lower crust bottom; M = mantle; A = asthenosphere; IC = inviscid core).

Layer	Depth (km)	ρ (kg dm^{-3})	ν (Pa s)	μ (GPa)
UC	0–18.5	2.65	∞	32.5
LC	18.5–28.5	2.75	$1 \cdot 10^{18}$	33.7
			$0.75 \cdot 10^{19}$	
			$1 \cdot 10^{19}$	
			∞	
LCB	28.5–32.5	2.90	10^{18}	35.5
			∞	
A	32.5–80.0	3.39	10^{19}	73.5
M	32.5–2891	3.39	10^{21}	73.5
IC	2891–6372	10.93	–	–

Earth model, described in Table 1, consists of five layers including a purely elastic upper crust, a viscoelastic lower crust, the mantle or asthenosphere and the core.

The depths of the crustal layers and their elastic values have been taken from the average depths of the seismogenic crust and MOHO in the southern Apennine area (Mostardini & Merlini 1986), while the deeper layers are based on standard global Earth models. Viscosity in the lower crust has been varied from typical values of 10^{19} Pa s (Pollitz *et al.* 1998). In order to mimic the reduction of viscosity within the lower crust, and the decoupling between the lower crust and the mantle, as expected on the basis of strength reduction with depth for the continental lithosphere under extension (Lynch & Morgan 1987; Cosgrove 1997), a thin region of the bottom of the lower crust, LCB in Table 1, has been reduced by one order of magnitude with respect to the normal LC value of 10^{19} Pa s. Due to our simplified viscosity profile within the lower crust, only effective viscosity resulting from the volumetric average within the two viscoelastic layers characterizing the lower crust can be compared with post-seismic results from other tectonic environments (Pollitz *et al.* 1998, 2000). A standard mantle (M) of 10^{21} Pa s below the lower crust, does not predict any sizeable deformation over the time-scale of post-seismic deformation. In order to test a possible alternative relaxation model, characterized by relaxation occurring in the asthenosphere rather than in the lower crust, another model based on an elastic upper and lower crust and viscoelastic asthenosphere (A) of 10^{19} Pa s has been considered.

The assumed fault system, consisting of three normal subfaults, is shown in Fig. 1, including the three levelling lines considered in this study, namely CZT2 (black dots), CZT3 (blue dots) and IGM81 lines (red dots), measured immediately after the main shock and four years later; the thin curve in Fig. 1, starting from Eboli and routing to Grottaminarda through Potenza, represents the levelling line along which the co-seismic vertical displacement has been measured (Arca *et al.* 1983; De Natale *et al.* 1988). The surface projections of the three faults F1, F2 and F3 are also shown by the light grey. The fault parameters of this model, shown in Table 2, have been obtained by Pingue *et al.* (1993) from the inversion of co-seismic vertical displacements. The total seismic moment has been inferred from seismological and geodetic data; for the main fault F1 the seismic moment M_0 is fixed at 24.4×10^{18} Nm, at 2.5×10^{18} Nm for F2 and at 3.2×10^{18} Nm for F3. A pure normal faulting mechanism is considered for each fault. Slip on the three sub-faults has been considered homogeneous, as assumed by Pingue *et al.* (1993), in our initial tests. Subsequently, while maintaining constant the seismic moment to $M_0 = 3.0 \times 10^{19}$ Nm, the slip distribution on the faults is varied with depth in order to reduce the misfit between model predictions and co-seismic observations.

Table 2. L1: fault length. L2: fault width along slip direction. Top: depth of fault top margin. Disl.: mean dislocation. Str.: strike.

Sub Event	L1 (km)	L2 (km)	Top (km)	Disl. (cm)	Str. (°)	Dip (°)
F1(0 s)	25	20	1.0	150	317	60
F2(18 s)	22	14	1.0	25	310	20
F3(40 s)	13	10	1.3	75	120	85

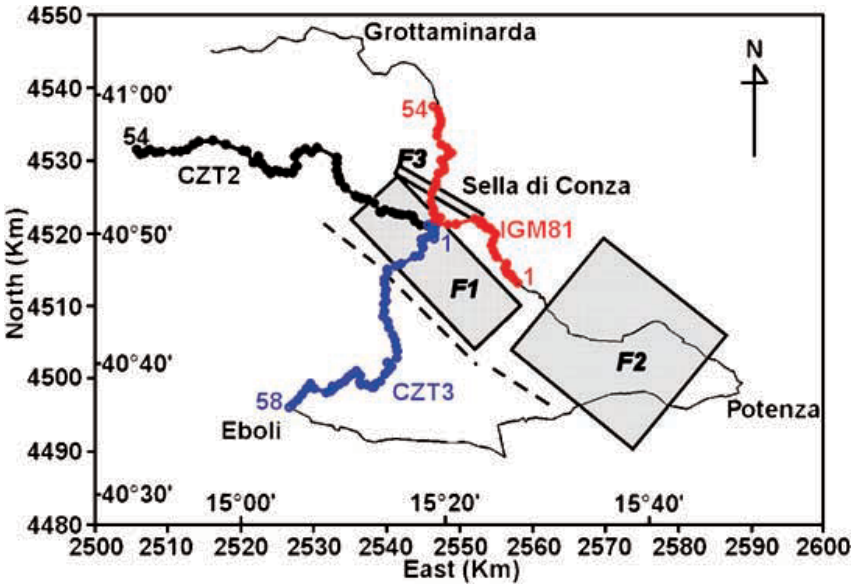

Figure 1. Fault model of the Irpinia 1980 earthquake. The levelling lines IGM81 (red), CZT2 (black) and CZT3 (blue) are also indicated. F1, F2 and F3 indicate the three faults, at 0 s, 18 s and 40 s respectively, as given in Table 2; the dashed lines provide the surface evidence of the faults. The first (1) and last (54, 58) benchmark of each levelling line are also shown.

3 MODELLING RESULTS

Fig. 2 shows the observed displacements along the levelling lines of Fig. 1, where the black vertical bars reproduce the observations and their average errors; post-seismic data sets, collected along the three high-precision, double runned levelling lines, were processed in the same way of co-seismic ones (Arca *et al.* 1983). The color curves represent the modelled vertical displacements due to viscoelastic relaxation without the co-seismic component, computed for various combinations of slip distribution and viscosities. In order to carry out a comparison independent from the choice of the zero in the levelling, each model result has been uniformly shifted in such a way that the mean residual vanishes; this shift also accounts for long wavelength contributions, such as regional tectonic uplift, that could be considered nearly constant in the epicentral area.

The red curves correspond to the reference model characterized by a uniform distribution of the seismic moment over the fault and by a lower crust viscosity of 10^{19} Pa s (Table 1, LC layer). The trends shown by this model agree with some basic features of the three lines, such as the subsidence along the points 1–20 of IGM81. However, the model does not predict the general uplift along CZT2, the uplift (order 20–30 mm) between the points 1–50 of CZT3 and the large gradient in the uplift at the point 20 of IGM81.

In order to increase the upwarping of the crust along CZT3, where this line crosses the major fault, it is necessary to investigate the distribution of slip along the faults, since relaxation response depends strongly on source depth. Inversion of co-seismic signal, controlled by the elastic properties of the medium, allows us to find a distribution that is independent from viscous parameters driving the post-seismic behaviour. The best fit seismic moment distribution is chosen by minimizing the L^1 norm of the residuals between co-seismic observations and model predictions for all the three lines simultaneously, and we find that the maximum slip occurs at depths of about 10 km, as shown in Table 3. This change in the post-seismic model results in the green curves of Fig. 2. The long wavelength uplift between the points 1–35 of CZT3 increases with respect to the red curve to 12 mm; the same is true along the profile CZT2 for the points 1–25, where uplift reaches 10 mm. Particularly evident is the model's ability to reconcile the change from subsidence into uplift along IGM81 from the benchmarks 15 to 35.

The fit between the observations and model results can be further substantially improved by reducing the viscosity in the lower crust from 10^{19} Pa s to 0.75×10^{19} Pa s, as shown in Table 1 for the LC layer, in the case of a non uniform seismic moment distribution. These results are given by the blue curves. The increase to 23 mm in the maximum displacement along CZT3 is accompanied by an increase to 15 mm and 10 mm along CZT2 and IGM81 respectively. Lowering the viscosity of the whole lower crust to 10^{18} Pa s can be excluded, since it would cause a maximum uplift of 12.8 cm, instead of the observed value of about 3 cm.

The general trend of observed displacements is well reproduced by the best fit model, except for some high frequency signals at very localized zones and a rather systematic underestimation of displacements in the northernmost zone of the IGM81 line. In order to explore alternative viscous models, the magenta curves in Fig. 2 are generated from a model with postseismic relaxation in the weak part of the upper-mantle, the asthenosphere, where the viscosity is fixed at 10^{19} Pa s (A layer, Table 1) and the slip distribution is given in Table 3. For all the three profiles, relaxation in the asthenosphere amplifies the signal with respect to crustal relaxation, due to the larger volume of material involved in the flow; asthenospheric relaxation introduces a long wavelength component in the

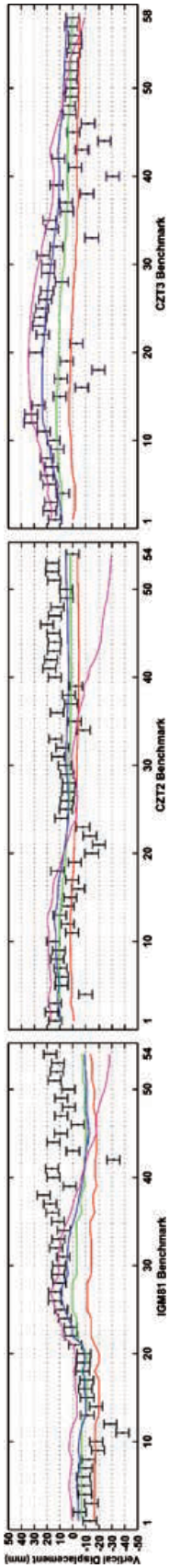

Figure 2. Levelling data for the three lines and modelling results: the red curves correspond to a transition zone viscosity of 10^{19} Pa s and uniformly distributed seismic moment, the green ones to the same viscosity but disomogeneous seismic moment accordingly to Table 3. The blue curves correspond to a lower crust (LC) viscosity of 0.75×10^{19} Pa s, and the seismic moment distribution of Table 3. The magenta curves stand for asthenospheric relaxation (A layer, Table 1) with purely elastic lower crust and seismic moment as in Table 3.

Table 3. Seismic moment distribution along the fault width (L2); M = $M_0/5$ where M_0 is given in the text; the fault description is given in Table 2.

Fault fraction	F1	F2	F3
1/5	0.8 × M	2.0 × M	2.0 × M
2/5	1.2 × M	2.0 × M	2.0 × M
3/5	1.5 × M	1.0 × M	1.0 × M
4/5	1.0 × M	0.0 × M	0.0 × M
5/5	0.5 × M	0.0 × M	0.0 × M

deformation, as shown by the conspicuous subsidence at large distance from the fault system, especially for the IGM81 and CZT2 profiles. This effect reflects the broadening, with respect to lower crust relaxation, of the deformation pattern around the major fault F1; this broadening is caused by relaxation at greater depths, within the weak upper-mantle (Pollitz *et al.* 2000). The peak-to-peak deformation evident in the magenta curves is larger than the observed and this suggests that the most appropriate relaxation model is the lower crust one; however, some of the characteristic features of the levelling lines, such as the change from subsidence to uplift for the IGM81 profile and the broad uplift of profile CZT3, are also reconciled by asthenospheric relaxation.

Fig. 3 shows the modelled co-seismic displacement based on the redistributed moment slip over the faults (red) superimposed on the geodetic inference from Pingue & De Natale (1993) (black). The co-seismic vertical displacement shows a rather complex pattern, due to the geometry of the levelling line, and resembles well the observed co-seismic data: the smooth decrease from −300 mm to −800 mm is due to the passing of the levelling line across the large hangingwall region of subsidence along the major fault F1; the steep increase from −800 mm to +100 mm is due to the combined effect of F1 and F3, when the line leaves the hangingwall region of the two faults and enters the footwall of F2.

Fig. 4 provides an areal view of the post-seismic vertical displacement accumulated in the period 1981–1985. The characteristic zones of uplift and subsidence of a normal fault event appear also in the post-seismic pattern of Fig. 4(a). This pattern shows the vertical deformation generated by the fault with viscosity model used in Fig. 2 and characterized by lower crust relaxation (blue curves, best-fit model). Two major features are noticeable: the broadness of the area affected by subsidence and uplift, and the reduction in the amplitude of the displacement, with a reduction of about a factor twenty with respect to the co-seismic displacements. Both effects are indicative of stress release at depth, and of the ability of the viscoelastic part of the crust to channel the flow at large distances from the fault. The expected present day peak-to-peak post-seismic vertical displacement, 22 yr after the earthquake, is 120 mm, characterized by the pattern of Fig. 4(a).

Fig. 4(b) shows the post-seismic deformation pattern in the same period as in Fig. 4(a), for relaxation in the asthenosphere and a purely elastic lithosphere, thus providing an areal view of the pattern responsible for the displacement given by the magenta curves in Fig. 2. These results, in comparison with Fig. 4(a), show the broadening of the deformation pattern with respect to the case of lower crust relaxation. The peak-to-peak vertical displacement is reduced from the 46 mm of Fig. 4(a) to 24 mm; particularly evident is a significant increase in the distance between the two uplifting and subsiding domes. The broadening and smoothing of the vertical displacement pattern is due to the combined flexural properties of the thick elastic lithosphere and relaxation involving the asthenosphere, both acting in concert to induce a long wavelength deformation component.

4 DISCUSSION AND CONCLUSIONS

Theoretical modelling of the post-seismic displacements in the area of the 1980 Irpinia earthquake indicates that observed displacements are generally in agreement with post-seismic viscoelastic predictions. This result is the first evidence of such deformations in the case of a large normal fault earthquake. Our modelling of the earthquake areas indicates that the effective average viscosity of the lower crust is 0.6×10^{19} Pa s. This inference agrees with the 'normal' lower crust viscosity of 10^{19} Pa s obtained by Pollitz *et al.* (1998) from post-seismic relaxation following the 1989 Loma Prieta earthquake: the 40 per cent discrepancy in the lower crust viscosity is not surprising given the different extensional environment considered in this study. Our results are also an indirect validation of the assumed depth and thickness of the lower crust. The characteristic wavelength of the post-seismic deformation in the Irpinia area supports evidence for viscoelastic relaxation occurring within the lower crust rather than in the uppermost part of the mantle; this contrasts with the 1992 Landers earthquake, where there are indications that relaxation also involves a weak upper-mantle (Pollitz *et al.* 2000). We find that a higher slip concentration at a depth ∼10 km provides a best fit to the observed data. A higher slip patch at similar depths was also inferred by De Natale (1989), from heterogeneous slip inversion of co-seismic vertical displacements. High slip concentrations on the main fault around 10 km of depth also correlate well with the main clusters of aftershocks, resulting mainly from off-fault events, triggered by Coulomb stress increase due to main faults dislocation (Troise *et al.* 1998). Strong correlation between high slip patches and neighboring earthquakes is expected in the

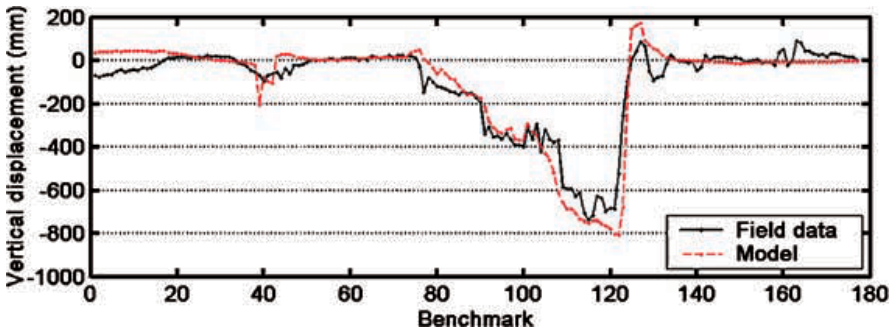

Figure 3. modelling results (black line) superimposed to the levelling lines measurement (red line) for the co-seismic vertical displacement, in mm. The fault parameters are those corresponding to the blue curves of Fig. 2.

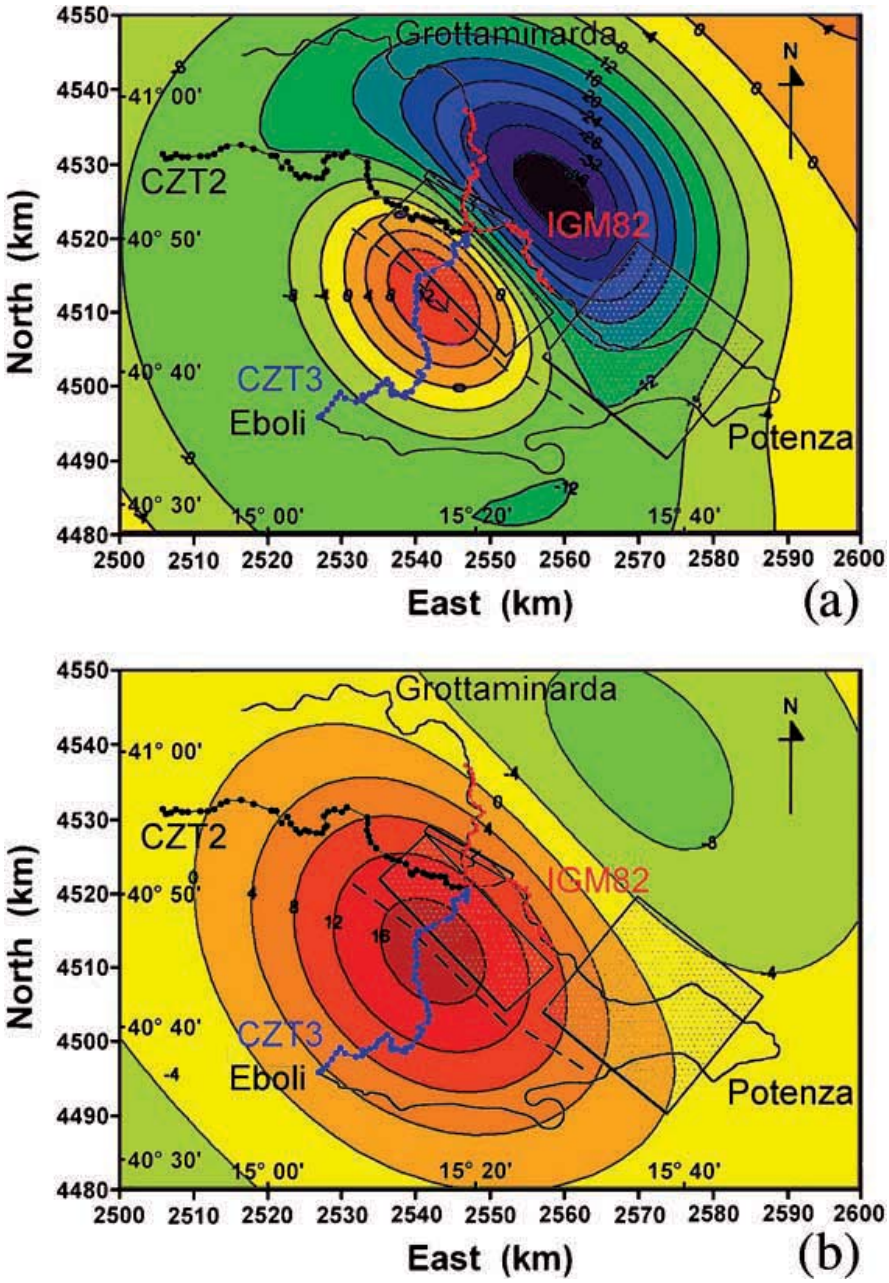

Figure 4. Modelling results superimposed to the levelling lines and faults of Fig. 1; panel 4a corresponds to the post-seismic displacement accumulated in the period 1981–1985 (in mm) due to crustal relaxation; fault parameters and lower crust viscosity are those corresponding to the blue curves of Fig. 2; panel 4b represents the post-seismic displacement in the same period of panel 4a due to asthenospheric relaxation; parameters are those corresponding to the magenta curves of Fig. 2.

framework of a Coulomb stress off-fault triggering, whereas an inverse correlation is expected for in-fault aftershocks, occurring at unbroken zones during the main shocks. The evidence for high slip concentration at depth from this study thus supports the results obtained by Troise *et al.* (1998) regarding the genesis of aftershocks of the Irpinia earthquake. The general trend of vertical displacements, and the maximum peak-to-peak amplitude, are well interpreted by viscoelastic relaxation; however, some unmodelled features of very localized subsidence or high frequency signals probably indicate the effect of other post-seismic deformation mechanisms, for example aftershocks (an aftershock which occurred in 1983 could be responsible for the subsidence in CZT3 profile, benchmarks 15–20), afterslip or fluid migration, acting locally in the period 1981–1985.

ACKNOWLEDGMENTS

This work is supported by the Italian Ministry of Instruction, University and Research COFIN2002 project 'A multidisciplinary monitoring and multiscale study of the active deformation in the northern

sector of the Adria plate'. We thank J. Mitrovica and an anonymous reviewer for their suggestion and constructive criticism.

REFERENCES

Arca, S., Bonasia, V., Gaulon, R., Pingue, F., Ruegg, J.C. & Scarpa, R., 1983. Ground movements and faulting mechanism associated to the 23 November, 1980, southern Italy earthquake, *Bollettino di Geodesia e Scienze Affini,* **XLII,** No. 2.

Bernard, P. & Zollo, A., 1989. The Irpinia (Italy) 1980 earthquake: detailed analysis of a complex normal faulting, *J. geophys. Res.,* **94,** 1631–1648.

Cosgrove, J. W., 1997. The influence of mechanical anisotropy on the behaviour of the lower crust, *Tectonophysics,* **280,** 1–14.

De Natale, G., 1989. Inversion of ground deformation data for variable slip fault models, *Software for Engineering Workstations,* **5,** 140–150.

De Natale, G., Pingue, F. & Scarpa, R., 1988. Seismic and ground deformation monitoring in the seismogenetic region of Southern Apennines, Italy, *Tectonophysics,* **152,** 165–178.

Lynch, H.D. & Morgan, P., 1987. The tensile strength of the lithosphere and the localization of extension, in *Continental Extensional Tectonics, Geological Society Special Publication,* eds, Coward, M.P., Dewey, J.F. & Hancock, P.L., **28,** 53–65.

Mostardini, P. & Merlini, S., 1986. Appennino centro-meridionale: sezioni geologiche e proposta di modello strutturale, *Mem. Soc. Geol. Ital.,* **35,** 177–202.

Pantosti, D. & Valensise, G., 1990. Faulting mechanism and complexity of the 23 November 1980, Campania-Lucania, earthquake, inferred from surface observations, *J. geophys. Res.,* **95,** 15 319–15 341.

Piersanti, A., 1999. Post-seismic deformation in Chile: constraints on the asthenospheric viscosity, *Geophys. Res. Lett.,* **26,** 3157–3160.

Pingue, F. & De Natale, G., 1993. Fault mechanism of the 40 s subevent of the 1980 Irpinia (Southern Italy) earthquake from levelling data, *Geophys. Res. Lett.,* **20,** 911–914.

Pingue, F., De Natale, G. & Briole, P., 1993. modelling of the 1980 Irpinia earthquake: constraints from geodetic data, *Annali di Geofisica,* **36, 1,** 27–40.

Pollitz, F.F., Burgmann, R. & Segall, P., 1998. Joint estimation of afterslip rate and post-seismic relaxation following the 1989 Loma Prieta earthquake, *J. geophys. Res.,* **103,** 26 975–26 992.

Pollitz, F.F., Peltzer, G. & Burgmann, R., 2000. Mobility of continental mantle: evidence from postseismic geodetic observations following the 1992 Landers earthquake, *J. geophys. Res.,* **105,** 8035–8054.

Riva, R.E.M. & Vermeersen, L.L.A., 2002. Approximation method for high-degree harmonics in normal mode modelling, *Geophys. J. Int.,* **151,** 309–313.

Troise, C., De Natale, G., Pingue, F. & Petrazzuoli, S., 1998. Evidence for earthquake interaction in South-Central Apennines (Italy) through static stress variations, *Geophys. J. Int.,* **134,** 809–817.

Westaway, R. & Jackson, J., 1984. Surface faulting in the Southern Italy Campania-Basilicata earthquake of the 23 November 1980, *Nature,* **312,** 436–438.